WPEDU-PR(18) 21167

D Brunetti et al.

Helical equilibrium MHD flow effects on the stability properties of low-n ideal modes in weak shear tokamak configurations

Preprint of Paper to be submitted for publication in
Plasma Physics and Controlled Fusion

This work has been carried out within the framework of the EUROfusion Consortium and has received funding from the Euratom research and training programme 2014-2018 under grant agreement No 633053. The views and opinions expressed herein do not necessarily reflect those of the European Commission.

Helical equilibrium MHD flow effects on the stability properties of low-n ideal modes in weak shear tokamak configurations

D. Brunetti,[1,*] J. P. Graves,[2] E. Lazzaro,[1] A. Mariani,[1] S. Nowak,[1] W. A. Cooper,[2] and C. Wahlberg[3]

[1]Istituto di Fisica del Plasma IFP-CNR, Via R. Cozzi 53, 20125 Milano, Italy
[2]École Polytechnique Fédérale de Lausanne (EPFL), Swiss Plasma Center (SPC), CH-1015 Lausanne, Switzerland
[3]Department of Astronomy and Space Physics, EURATOM/VR Fusion Association,
P.O. Box 515, Uppsala University, SE-751 20 Uppsala, Sweden

(Dated: September 4, 2018)

The impact of equilibrium helical flows on the stability properties in low-shear tokamak plasmas is assessed. The corrections due to such helical flow to the equilibrium profiles (mass density, pressure, Shafranov shift, magnetic fluxes) are computed rigourously by minimising order by order the generalised Grad-Shafranov equation. By applying the same minimisation procedure, a set of three coupled equations, suitable for the study of magnetohydrodynamic perturbation localised within core or edge transport barriers is derived in circular tokamak geometry. These equations are then used to analyse the stability of infernal modes localised within the edge pedestal transport barrier.

Tokamak H-mode configurations are characterised by an enhanced energy confinement time which makes this operation regime the reference one for the next generation tokamaks. H-mode tokamak plasmas are characterised by strong edge pressure gradients (due to both temperature and density), which favour the formation of short wavelength modes called Edge Localised Modes (ELMs) [1]. These events are of extreme concern because high energy and particle loads are deposited on the plasma facing components (in particular the divertor target plate). Thus in the last decades an increasing interest grew on the development of techniques able to mitigate or entirely suppress ELMs. ELM control has been achieved by acting on the plasma externally by applying, e.g. resonant magnetic perturbations [2] or by injecting pellets [3]. Since all these (active) techniques involve an external action, recent studies focussed on the possibility of the existence of naturally ELM free high performance scenarios (passive ELM control).

One of these intrinsically ELM-free operating scenarios is the so called quiescent high confinement (QH) regime [4, 5]. QH plasmas operate at low edge collisionality ($\nu^* < 0.3$ [6]) and are characterised by large edge pressure gradients (edge transport barrier, with also a discrete core transport barrier [7]) and high energy confinement time, features typical of the standard H-mode regime, but without the dangerous presence of ELMs. Indeed it has been observed [6, 8, 9] that ELMs are replaced by a new kind of instability called edge harmonic oscillation (EHO). Interestingly EHOs are always observed during the QH-mode operation [4, 6, 9, 10]. Such instabilities are low-n (e.g. $n = 1, m = 4, 5$ while ELMs in contrast are characterised by large n values) magnetohydrodynamic (MHD) oscillations whose associated energy loads on the materials facing the plasma are much lower compared to regimes where ELMs are present. Indeed the edge particle transport is enhanced by EHOs, and this allows a steady density control and ash removal without the impulsive energy bursts typical of ELMs [6, 11].

A possible candidate for the explanation of the appearance of these perturbations could be kink-peeling (KP) modes. KP modes are perturbations localised near the plasma edge driven by the combined action of current gradients (kink part) and edge pressure gradients (ballooning part) [12]. A mainly current driven KP mode is dominated by a single Fourier harmonic. If the edge pressure gradient is increased, due to poloidal coupling a larger number of sideband harmonics accompanying the dominant mode can be excited. If the pressure gradient is increased further eventually a ballooning-like behaviour is expected. Linear and nonlinear simulations of QH-mode DIII-D plasma discharges with ideal and resistive wall boundary conditions showed that KP modes can develop, allowing low-n modes ($n = 1, 2$) to saturate forming three dimensional stationary equilibria. Although moderately large-n KP modes are the most unstable during the linear phase, their nonlinear interplay allows low-n harmonics to be dominant during the nonlinear stage [13]. It has also been recently discovered that equilibrium $\boldsymbol{E} \times \boldsymbol{B}$ flows favour the growth of low-n modes, while short wavelength harmonics are damped [14, 15]. Three dimensional free boundary MHD equilibria simulations of JET-like plasmas, with a locally flat safety factor computed consistently with the associated pressure gradients, recovered edge saturated ideal KP structures (driven mainly by non axisymmetric components of the parallel current density) [16, 17] which lead to a dominant $n = 1$ corrugated boundary.

In the low collisionality regime, large bootstrap contributions may rise in the region of large pressure gradients. Having large bootstrap contributions causes in turn a plateau in the safety factor q profile (this in particular can occur in proximity of the plasma boundary if strong edge transport barriers are present). In these conditions, i.e. large pressure gradients and q flat over and extended region, it is likely that *infernal-type* instabilities may develop. Infernal modes are characterised by a toroidicity induced (due to pressure gradients) coupling between neighbouring Fourier harmonics, so that the fluid perturbation is characterised by a main mode of poloidal mode number m accompanied by its $m \pm 1$ sidebands. Indeed recent numerical studies of low-n MHD modes in the QH-mode with a plateau in q near the edge, corresponding to the peak of the

* Electronic address: brunetti@ifp.cnr.it

bootstrap current, have been found to have *infernal-like* features [18–20]. In addition, the linear and nonlinear stability analysis of DIII-D QH-mode discharges affected by the presence of EHOs (low-n, with $m = 3, 4, 5$ located close to the edge) showed resemblance to infernal type perturbations [21]. It is also interesting to note that in absence of $\boldsymbol{E}\times\boldsymbol{B}$ flows, the linear growth rate increases linearly with the toroidal number n [13–15, 19], a feature which is typical of infernal modes.

Thus the main aim of this work is to extend the analysis presented in Refs. [22, 23], with the additional ingredient of an equilibrium helical flow, investigating, in particular, the effect of its equilibrium poloidal component on the stability properties of MHD modes. The key ingredient for our analysis is the presence of a local flattening of the safety factor, in proximity of a rational surface. At this region, supposed sufficiently narrow, the presence of sufficiently strong pressure gradients allows mode coupling. Hence the first objective of our analysis is derive a set of MHD equations in weak shear and strong pressure gradients with the inclusion of equilibrium helical flows, suitable for the analysis of transport barriers, either internal (ITB) or at the edge (ETB) where strong density or temperature (or both) gradients are expected. Thus the analysis of the perturbation behaviour is split into two regions, one in which the magnetic shear is large and the Fourier modes behave independently and a weak shear region in which an *infernal*-type coupling, i.e. only between neighbouring sidebands, occurs. The resulting equations are then employed for analysing the behaviour of low-n ($n \sim 1$) pressure driven MHD modes either in the core plasma (ITB) or at the edge (ETB). Matching conditions for the fluid displacements at the boundaries of the weak shear region (either at the edge for ETBs or within the plasma for ITBs) determine the perturbation behaviour, i.e. it is specified whether we are analysing ETBs or ITBs. The procedure yields eventually a dispersion relation which is then used to compute the growth rate, identifying stable (or unstable) parameters domain.

Hence the paper is organised as follows. Section I describes the geometry considered and the physical model employed. The profiles of the equilibrium quantities (i.e. magnetic fluxes, mass density, pressure etc.) are rigorously derived by solving the force balance equation in presence of helical flows. The resulting expressions for the plasma shaping factors and the related metric tensor coefficients are then evaluated. Section II is devoted to the derivation of the equations for the perturbation. The mode spectrum of the perturbation assumes the presence of a main mode of helicity m/n accompanied by neighbouring sidebands $m \pm 1$ and $m \pm 2$. The analysis, carried out within the Frieman-Rotenberg framework, consists in minimising order by order the appropriate projections of the momentum equation. This eventually yields a set of three coupled differential equations with an *infernal* structure (i.e. inertia enters only in the equation for the dominant mode over a fairly extended region). A discussion their validity on the applicability to our problem is given. In section III the eigensolutions for three Fourier harmonics (i.e. the m and $m \pm 1$ modes) are solved for a particular choice of safety factor and pressure profiles, focussing in particular to edge transport barriers (i.e. pedestal relevant configurations). The boundary conditions at the plasma frontier are left unspecified, so that the treatment can be generalised to different configurations. Nevertheless the crucial stabilising influence of the sheared poloidal flow is well established in the two different regimes of highly localised low-m and short wavelength (i.e. large m) perturbations. Finally the findings of this work and future outlook are summarised in section IV. The appendices provide the exact expressions to higher orders of the metric tensor and a detailed derivation of the dispersion relation when the approach described in the body of the paper is applied to assess the MHD stability of internal transport barriers.

I. PHYSICAL MODEL AND EQUILIBRIUM

We analyse a large aspect ratio tokamak configuration of major and minor radii R_0 and a respectively ($\varepsilon = a/R_0 \ll 1$) with shifted circular toroidal surfaces. We use a coordinate system (r, θ, φ) where r is a flux label with the dimensions of length, θ and φ are the poloidal and toroidal angles respectively (the parametrisation of the flux surfaces will be described later). The contravariant and covariant basis vectors are denoted respectively by $(\boldsymbol{\nabla} r, \boldsymbol{\nabla}\theta, \boldsymbol{\nabla}\varphi)$ and $(\boldsymbol{e}_r, \boldsymbol{e}_\theta, \boldsymbol{e}_\varphi)$. At the equilibrium a strong toroidal field (B_T) and a smaller poloidal field (B_P) with $B_P/B_T \sim O(\varepsilon)$ are assumed. The ratio of the kinetic pressure over the magnetic pressure is assumed small, i.e. $\beta = p/B_T^2 = \beta \sim O(\varepsilon^2)$ where p is the pressure. The stability analysis is based on the single fluid ideal MHD equations [24, 25]:

$$\rho\left[\partial_t \boldsymbol{v} + \boldsymbol{v}\cdot\boldsymbol{\nabla}\boldsymbol{v}\right] = -\boldsymbol{\nabla} p + \boldsymbol{J}\times\boldsymbol{B}, \tag{1}$$

$$\boldsymbol{E} + \boldsymbol{v}\times\boldsymbol{B} = 0, \tag{2}$$

$$\partial_t p + \boldsymbol{v}\cdot\boldsymbol{\nabla} p + \Gamma p \boldsymbol{\nabla}\cdot\boldsymbol{v} = 0, \tag{3}$$

$$\partial_t \rho + \boldsymbol{\nabla}\cdot(\rho\boldsymbol{v}) = 0, \tag{4}$$

$$\partial_t S + \boldsymbol{v}\cdot\boldsymbol{\nabla} S = 0, \tag{5}$$

$$p = S(r)\rho^\Gamma \tag{6}$$

where $\boldsymbol{v}$ is the plasma MHD velocity, ρ the mass density, p the plasma pressure, $\boldsymbol{J} = \boldsymbol{\nabla}\times\boldsymbol{B}$ (having normalised $\mu_0 = 1$), Γ is the adiabatic index and $\boldsymbol{E}$ the electric field. The quantity S is related to the specific entropy and the last expression of the set above is the equation of state. In the following section, the expressions of the various equilibrium quantities are calculated, providing a complete characterisation of the equilibrium.

A. Equilibrium profiles

Let us now set ourselves at the equilibrium and analyse the set of the equations (1)-(6) in axisymmetric tokamak geometry. In addition to the shape of the zeroth orders of the total helical MHD flow, the equilibrium is specified by imposing two additional external functions: in our case the zeroth orders plasma pressure and toroidal current. We denote equilibrium quantities with the subscript eq. For a generic equilibrium scalar quantity G_{eq} we set $\partial_t G_{eq} = 0$ and because of

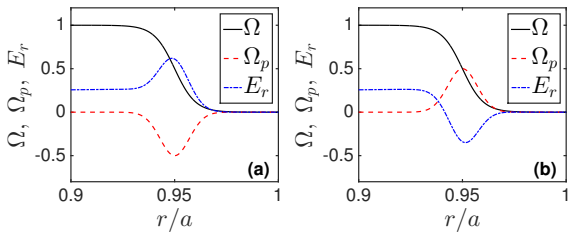

Figure 1. Example of edge toroidal (Ω) and poloidal (Ω_p) flow profiles and the resulting equilibrium (covariant) radial electric field, for a negative (a) and positive (b) Ω_p with a flat $q = 3.5$ (the magnetic field on the axis B_0 has been normalised to unity). Note that in this example the toroidal flow is taken with positive sign. If the sign of Ω is flipped, we must swap E_r between (a) and (b) changing its sign.

axisymmetry, we have also $\partial_\varphi G_{eq} = 0$. The magnetic field in the plasma is represented as [26]:

$$\boldsymbol{B}_{eq} = T\boldsymbol{\nabla}\varphi - \boldsymbol{\nabla}\psi_{eq} \times \boldsymbol{\nabla}\varphi, \tag{7}$$

where $\psi_{eq} = \psi_{eq}(r)$ so that we immediately have that $B^r_{eq} = 0$ (we use the notation $B^2_{eq} = B^\theta_{eq} B_{\theta eq} + B^\varphi_{eq} B_{\varphi eq}$). By writing $\boldsymbol{E}_{eq} = -\boldsymbol{\nabla}\Phi$ where Φ is the electrostatic potential, from the projection of the Ohm's law along $\boldsymbol{B}_{eq}$ we have that Φ is a flux function. Assuming an equilibrium flow $\boldsymbol{v}_{eq}$ of order ε with respect to the Alfvén frequency $\omega_A (= B_0/(R_0\sqrt{\rho_{eq}})$, where B_0 is the value of the magnetic field on the axis), the projection of (2) along the covariant poloidal and toroidal directions gives $v^r_{eq} = 0$ (i.e. no equilibrium flow across the magnetic surfaces). Equation (4), which at equilibrium is written as $\boldsymbol{\nabla}\cdot(\rho_{eq}\boldsymbol{v}_{eq}) = 0$, after introducing an appropriate generic flux function A eventually yields:

$$v^\vartheta_{eq} = B^\theta_{eq}\frac{A(r)}{\rho_{eq}}.$$

Thus after inserting the equation above in the covariant radial projection of (2) we get:

$$v^\varphi_{eq} = \Omega(r) + B^\varphi_{eq}\frac{A(r)}{\rho_{eq}},$$

where $\Omega(r)$ is an arbitrary flux function. Hence the expression for the equilibrium flow is given by [25]:

$$\boldsymbol{v}_{eq} = R^2\Omega\boldsymbol{\nabla}\varphi + \boldsymbol{B}_{eq}\frac{A(r)}{\rho_{eq}}. \tag{8}$$

We shall introduce the quantity $\Omega_p = A(r)B_0/(\rho_0 R_0)$, which represents the poloidal rotation frequency (in our assumptions $\Omega \sim \Omega_p$). Focussing on the edge region an example of the equilibrium helical flow (both toroidal and poloidal components) and the associated electric field computed by Eq. (2) is shown in figure 1 (an example of the shape of the edge radial electric field can be found in Refs. [6, 27]).

Using the expression above in equation (5) gives $S_{eq} = S_{eq}(r)$. From the covariant toroidal projection of (1) we obtain:

$$T = \frac{1}{1 - A^2/\rho_{eq}}\left[F(r) + R^2 A\Omega\right], \tag{9}$$

with $F(r)$ being an arbitrary flux function of order $1/\varepsilon$ to be determined. Finally the poloidal covariant projection of the equilibrium momentum equation, by means of (6), provides the equation for the density, i.e.:

$$\frac{1}{2}\left(\frac{B_{eq}A}{\rho_{eq}}\right)^2 - \frac{1}{2}R^2\Omega^2 + \frac{\Gamma}{\Gamma-1}S_{eq}\rho^{\Gamma-1}_{eq} = H(r), \tag{10}$$

where $H(r)$ is an arbitrary function. From (9) and (10), it is immediate to recognise that ρ (and thus p) and T are, in general, functions both of the radial and poloidal variables. In order to determine the expressions for the mass density and the covariant toroidal field, we first parametrise in the (r, θ, φ) coordinate system the flux surfaces by approximating $R = R_0 + r\cos\theta$ and $Z = r\sin\theta$: these are used to compute the leading order expressions of the metric tensor, which read $g_{rr} = 1$, $g_{\theta\theta} = r^2$, $g_{r\theta} = 0$ and $\sqrt{g} = rR_0$. The mass density profile is written as a power series in ε, viz. $\rho_{eq} = \rho_0(r) + \varepsilon\rho_1(r,\vartheta) + \ldots$. By performing an ε expansion of equation (9), it is easy to see that the first three ε-terms of F are flux quantities, thus we write $F = R_0 B_0(1 + O(\varepsilon^2))$ (this approximation will be checked *a posteriori*). Plugging these quantities in the θ derivative of (10) and performing a series expansion in ε (similarly to what has been done in Ref. [28] though with slightly different results) we obtain the expression for the first order correction to the mass density, namely:

$$\frac{\rho_1}{\rho_0} = \frac{r}{R_0}\left(\frac{\Omega^2 + \Omega_p^2}{\Gamma\omega_A^2\beta_0 - \Omega_p^2}\right)\cos\theta, \tag{11}$$

where $\beta_0 = p_0/B_0^2$ with $p_0 = S_{eq}\rho_0^\Gamma$ which is an externally imposed function which, among with the total current distribution, determines the equilibrium profiles and plasma shaping (we point out that the Alfvén frequency is function of the minor radius through the equilibrium mass density). Introducing the Mach numbers $\mathcal{M}_T^2 = \frac{\Omega^2}{\Gamma\omega_A^2\beta_0}$ and $\mathcal{M}_p^2 = \frac{\Gamma\Omega_p^2}{\omega_A^2\beta_0}$, the first order correction to the mass density becomes $\rho_1 = \frac{\rho_0 r}{R_0}\left(\frac{\mathcal{M}_T^2 + \mathcal{M}_p^2}{1-\mathcal{M}_p^2}\right)\cos\theta$. A singularity in the density profile (shock) appears when $\mathcal{M}_p = 1$ [25, 28], hence we assume in our analysis to operate always with $\mathcal{M}_p < 1$ (below the shock boundary). For sake of clarity for the calculations presented in Sec. II we write $\rho_1 = \frac{\rho_0 r}{R_0} f\cos\theta$ with $f = \left(\frac{\mathcal{M}_T^2 + \mathcal{M}_p^2}{1-\mathcal{M}_p^2}\right)$.

To next order the mass density correction is written as $\frac{\rho_2}{\rho_0} = \varepsilon^2\left(g_a(r) + g_b(r)\cos^2\theta\right)$. Analogously, by employing (6) we can express the equilibrium pressure as a powers series in ε, i.e. $p_{eq} = p_0 + \varepsilon p_1 + \ldots$, where p_0 has been defined above and:

$$\frac{p_1}{p_0} = \frac{\Gamma\rho_1}{\rho_0}, \tag{12}$$

$$\frac{p_2}{p_0} = \varepsilon^2\left(f_a(r) + f_b(r)\cos^2\theta\right). \tag{13}$$

The exact expressions of the flux functions $g_{a,b}(r)$ and $f_{a,b}(r)$ do not play any role in the following analysis, and therefore they are not given.

We shall refer to the covariant radial component of (1) as the generalised *Grad-Shafranov* (GS) equation (in absence of helical flows this corresponds to the GS equation given in, e.g., Ref. [29]). We introduce the following parametrisation of the flux surfaces [29, 30]:

$$R = R_0 + r\cos\theta - \Delta - E\cos\theta - P\cos\theta, \tag{14}$$

$$Z = r\sin\theta + E\sin\theta - P\sin\theta, \tag{15}$$

where $\Delta(r) \sim a\varepsilon$ is the Shafranov shift, E is the elongation function with $E \sim a\varepsilon^2$ and $P \sim a\varepsilon^2$ is a convenient flux relabelling function. Note that triangularity effects have been neglected and the analysis is performed in a nearly circular geometry (i.e. small elongation). The equilibrium poloidal flux is expanded in an ε series according to $\psi_{eq} = \psi_0 + \varepsilon\psi_1 + \varepsilon^2\psi_2 \ldots$, while $F = R_0 B_0(1 + \varepsilon^2 F_2 + \ldots)$. The GS equation is formally written as:

$$\sum_{n=0}^{\infty} \varepsilon^n \mathcal{U}_n = 0.$$

The parameters of the ε series expansion of the equilibrium quantities (i.e. ψ_{eq}, Δ, etc.) are found by setting to zero order by order the quantities $\mathcal{U}_n$. The first two orders are vanishing, namely $\mathcal{U}_0 = \mathcal{U}_1 = 0$. We introduce the safety factor function q defined as:

$$q = \frac{1}{2\pi}\int_0^{2\pi} d\theta \frac{B^{\varphi}_{eq}}{B^{\theta}_{eq}}.$$

This function, which is a supposed given parameter of the equilibrium, is related to the total toroidal current density. The rotational transform is defined as $\mu = 1/q$. From the definition above we immediately have $\psi_0 = rB_0/q$ and $\psi_1 = 0$. Choosing the following form for P [29, 30]:

$$P = \frac{r\Delta}{2R_0} + \frac{r^3}{8R_0^2}, \tag{16}$$

the expression for ψ_2 is then determined (although not used afterwards). Minimising the next order ($\mathcal{U}_2 = 0$) we obtain the leading order expression for $F = R_0 B_0(1 + F_2)$:

$$F = R_0 B_0\Big[1 - \frac{p_0}{B_0^2} - \frac{\Omega_p^2}{\omega_A^2} - \frac{\Omega\Omega_p}{\omega_A^2} - \int dr \frac{r}{R_0^2}\left(\frac{2-\hat{s}}{q^2}\right)\Big],$$

with $\hat{s} = rq'/q$. Proceeding further with the minimisation it is possible to show that the next order correction to F is vanishing (viz. $F_3 = 0$). By minimising the $\cos\theta$ component of $\mathcal{U}_3$ we obtain the equation for the Shafranov shift:

$$\Delta'' + \left(\frac{3}{r} - \frac{2q'}{q}\right)\Delta' - \frac{1}{R_0} + \frac{2rR_0 p'_{\Omega}}{(\psi'_0)^2} = 0 \tag{17}$$

with $p_\Omega = p_0[1 + (\frac{\Omega+\Omega_p}{\omega_A})^2/(2p_0)]$. Note that the magnetic axis shift is enhanced by the centrifugal effect of the total velocity in the toroidal direction, which contains both Ω and Ω_p contributions. Finally $\mathcal{U}_4 = 0$ provides an expression for ψ_3 and E both of which do not play a role in the following analysis.

The flux surfaces parametrisation is completely determined by Eqs. (16) and (17) and by the function E (although not explicitly determined). Hence in the following section the expression for the metric tensor is derived.

B. Metric tensor

We introduce a straight field line coordinate system (r, ϑ, φ) where r and φ are the flux label and toroidal angle already defined in the previous section, while ϑ is the poloidal-like angular variable which allows to "straighten" the magnetic field. In such a coordinate system the ratio $B^{\varphi}_{eq}/B^{\vartheta}_{eq}$ is a flux function. The *straightened* angle is related to the one given in the parametrisation (14) and (15) by the following relation:

$$\theta = \vartheta - \lambda_1(r,\vartheta) - \lambda_2(r,\vartheta) + \ldots,$$

where $\lambda_n(\sim \varepsilon^n)$ are periodic functions of their angular variable which are determined by setting to zero the oscillating part of $B^{\varphi}_{eq}/B^{\vartheta}_{eq}$. Hence the first two orders give:

$$\lambda_1 = -\left(\frac{r}{R_0} + \Delta'\right)\sin\vartheta,$$

$$\lambda_2 = -\left(\frac{r^2}{2R_0^2} + (\Delta')^2 + \frac{3r}{2R_0}\Delta' + E' - \frac{E}{r}\right)\frac{\sin 2\vartheta}{2}.$$

Using the expressions above the metric tensor elements, defined as $g_{ij} = \partial_i R\partial_j R + \partial_i Z\partial_j Z$, are readily computed to order ε^2 (below we explicitly write only the first order contributions):

$$\begin{aligned}
g_{rr} &= 1 - 2\Delta'\cos\vartheta + g_{11},\\
g_{r\vartheta} &= r\left(\frac{r}{R_0} + \Delta' + r\Delta''\right)\sin\vartheta + g_{12},\\
g_{\vartheta\vartheta} &= r^2 + 2r^2\left(\frac{r}{R_0} + \Delta'\right)\cos\vartheta + g_{22},\\
g_{\varphi\varphi} &= R_0^2(1 + \tfrac{2r}{R_0}\cos\vartheta) + g_{33},\\
\frac{1}{\sqrt{g}} &= \frac{1}{rR_0}(1 - \tfrac{2r}{R_0}\cos\vartheta) + J_2,
\end{aligned} \tag{18}$$

where g_{11}, g_{12}, g_{22}, g_{33}, J_2 are order ε^2 corrections whose expressions are reported in appendix A. Hence helical flow corrections enter in the metric tensor through the enhance Shafranov shift. We point out that the ε^2 corrections to g_{ij}, required in the calculation of the Jacobian, are necessary to obtain the right expressions in the following analysis (i.e. the Christoffel symbols). This is discussed in the next section.

II. STABILITY ANALYSIS

In this section we show the derivation for low frequency MHD modes, specifying afterwards the analysis to low-shear configurations. A strict aspect ratio expansion is performed similarly to previous works [31, 32], which are extended by the inclusion of poloidal flow effects. The new difficulty in our calculation arises due the presence of the poloidal flow which is a function both of the radial and angular variables (cf. (8)). A great deal of algebra is required for the following derivation, in which the approach of a rigorous direct expansion in the inverse aspect ratio is employed, thus we perform the analysis

helped by computer-aided algebra tools. Eventually a rather simple set of equation can be derived and simplified further invoking robust physical arguments.

Hereafter for sake of simplicity the equilibrium flow, mass density and magnetic fields are denoted by $\boldsymbol{v}$, ρ and $\boldsymbol{B}$ respectively. Following [33], we introduce the Lagrangian fluid displacement $\boldsymbol{\xi}$ defined by:

$$\tilde{\boldsymbol{v}} = \partial_t \boldsymbol{\xi} + \boldsymbol{v}\cdot\boldsymbol{\nabla}\boldsymbol{\xi} - \boldsymbol{\xi}\cdot\boldsymbol{\nabla}\boldsymbol{v},$$

where $\boldsymbol{v}$ is the equilibrium helical flow given by equation (8). The perturbation $\boldsymbol{\xi}$ is assumed to have a time dependence of the type $\exp(-i\omega t)$ where in general ω is complex. Hence by expressing $\tilde{\rho}$ and $\tilde{\boldsymbol{B}}$ as function of $\boldsymbol{\xi}$, the Frieman-Rotenberg eigenvalue equation for the mode frequency ω is derived [31, 32]:

$$\rho\omega^2\boldsymbol{\xi} + 2i\rho\omega\boldsymbol{v}\cdot\boldsymbol{\nabla}\boldsymbol{\xi} - \rho\boldsymbol{v}\cdot\boldsymbol{\nabla}[\boldsymbol{v}\cdot\boldsymbol{\nabla}\boldsymbol{\xi}] + \boldsymbol{\nabla}\cdot[\rho\boldsymbol{\xi}(\boldsymbol{v}\cdot\boldsymbol{\nabla})\boldsymbol{v}] + \boldsymbol{\nabla}(\phi + \boldsymbol{B}\cdot\boldsymbol{Q}) + \boldsymbol{B}\cdot\boldsymbol{\nabla}\boldsymbol{Q} + \boldsymbol{Q}\cdot\boldsymbol{\nabla}\boldsymbol{B} = 0, \tag{19}$$

where $\phi = \boldsymbol{\xi}\cdot\boldsymbol{\nabla}p + \Gamma p\boldsymbol{\nabla}\cdot\boldsymbol{\xi}$ and $\boldsymbol{Q} = \boldsymbol{\nabla}\times(\boldsymbol{\xi}\times\boldsymbol{B})$ represent respectively the perturbed pressure and magnetic field contributions. The term $\delta p = \Gamma p\boldsymbol{\nabla}\cdot\boldsymbol{\xi}$ represents the compressible contribution to the perturbed pressure. Terms of the form $\boldsymbol{\nabla}\boldsymbol{A}$ are evaluated by using the Christoffel symbols, namely (here $x = r, \vartheta, \varphi$) [26]:

$$\left(\frac{\partial \boldsymbol{A}}{\partial x^k}\right)_j = \frac{\partial A_j}{\partial x^k} - \Gamma^i_{jk}A_i,$$

$$\Gamma^i_{jk} = \frac{g^{im}}{2}\left[\frac{\partial g_{mj}}{\partial x^k} + \frac{\partial g_{mk}}{\partial x^j} - \frac{\partial g_{jk}}{\partial x^m}\right],$$

where the Einstein summation rule has been implicitly used. We may formally rewrite equation (19) conveniently normalised with respect to the Alfvén frequency as:

$$\boldsymbol{K}(\boldsymbol{\xi}) = 0. \tag{20}$$

We point out that the advantage of the Frieman-Rotenberg approach to the stability is the fact that all the perturbed quantities are written explicitly as function of the Lagrangian fluid displacement, thus allowing a direct expansion in terms of $\boldsymbol{\xi}$ (contrarily to the Eulerian approach in which, e.g., the perturbed magnetic field has implicit dependencies). This is particularly useful when equilibrium quantities depend upon the angular variable.

We assume that $\omega \sim \Omega \sim \Omega_p \sim \varepsilon\omega_A$ and $q \sim 1$. In addition we suppose that the perturbations analysed have poloidal and toroidal wave numbers of order unity. Applying the *infernal model*, a dominant mode of helicity m/n is assumed accompanied by its neighbouring $m \pm 1$ and $m \pm 2$ sidebands. Thus according to Ref. [31] the Lagrangian fluid displacement $\boldsymbol{\xi}$ is expanded as follows:

$$\xi^r = (\xi^r_m + \varepsilon^2\hat{\xi}^r_m)e^{i(m\vartheta - n\varphi)} + \varepsilon\sum_{m'=\pm1}\xi^r_{m+m'}e^{i[(m+m')\vartheta - n\varphi]} + \varepsilon^2\sum_{m'=\pm2}\xi^r_{m+m'}e^{i[(m+m')\vartheta - n\varphi]}.$$

Analogous expressions are employed for the ϑ and φ components of $\boldsymbol{\xi}$. The procedure to obtain the eigemode equation for the radial displacement ξ^r_m is described by the following steps: (i) first the $\boldsymbol{e}_\vartheta$ and $\boldsymbol{e}_\varphi$ projections of (19) are employed to specify $\xi^{\vartheta,\varphi}_\ell$ and $\hat{\xi}^r_m$ in terms of ξ^r_ℓ, (ii) the $m \pm 1$ components of the projection along $\sqrt{g}\boldsymbol{B}$ of (19) [34] provide an expression for the *compressible-like* contribution of the perturbed pressure (viz. the term $\Gamma p\boldsymbol{\nabla}\cdot\boldsymbol{\xi}$) which in turn yields the $2q^2$ Glasser-Greene-Johnson inertia enhancement factor [35], (iii) finally by applying the operator [34, 36]

$$\hat{\boldsymbol{L}} = \sqrt{g}\boldsymbol{\nabla}\varphi\cdot\boldsymbol{\nabla}\times\frac{1}{B^\varphi}$$

on (19) and selecting the m and $m \pm 1$ components we eventually obtain the complete set of coupled eigenvalue equations which will be used for the derivation of the dispersion relation.

The two leading orders (viz. ε^0 and ε) of the covariant φ projection of (20) ($\boldsymbol{K}_\varphi = 0$), regardless the strength of the magnetic shear, yield:

$$\xi^\vartheta_\ell = \frac{i}{r\ell}(r\xi^r_\ell)' + \mu\xi^\varphi_\ell, \quad \ell = m, m \pm 1. \tag{21}$$

A similar expression to the equation above is obtained for the $m \pm 2$ Lagrangian displacement by expanding further in ε the equation $\boldsymbol{K}_\varphi = 0$ and selecting the $m \pm 2$ Fourier mode. By taking the ε^2 order of the mth component of $\boldsymbol{K}_\vartheta$ and $\boldsymbol{K}_\varphi$ we obtain two equations involving $\xi^{r,\vartheta}_m$ and $\hat{\xi}^{r,\vartheta,\varphi}_m$. It is possible to show that by combining these two expressions, a single equation for ξ^φ_m as function of ξ^r_m can be obtained. This leads to:

$$\xi^\varphi_m = 0, \tag{22}$$

which together with (21) yields the usual perpendicular incompressibility condition. Hence inserting the expressions for the leading orders of the perturbed Lagrangian fluid displacement into the contravariant toroidal component of the perturbed magnetic field we obtain (B_0 denotes the valued of the magnetic field on the axis):

$$Q^\varphi = \frac{rB_0}{R_0^3}e^{i(m\vartheta - n\varphi)}\Big[\tfrac{n}{m}(\mu - \tfrac{n}{m})r\frac{d\xi^r_m}{dr} + \xi^r_m(2\mu^2 - \tfrac{n^2}{m^2} - \tfrac{n}{m}\mu + \frac{R_0^2}{r}\beta_0' - \mu^2\hat{s})\Big] + O(\varepsilon^4). \tag{23}$$

We stress the point that to this order no assumptions on the weakness (or strength) of the magnetic shear have been introduced, apart the usual condition that it does not exceed the ε^0 order.

Thus now we shall divide the analysis of Eq. (19) into two regions, one which is characterised by a magnetic shear of order of unity (*sheared region*), and the other in which $rq' \sim \varepsilon$ (*weak-shear region*). We point out that the equilibrium flow, with the ordering adopted in our analysis, has an appreciable effect only where the field line bending contribution is small. Therefore before proceeding further with the derivation of the stability equations in the weak shear region which turn out to require a great deal of algebra we shall focus for the moment on the high shear region, in which the derivation

of the eigenmode equations is simpler. Indeed if $rq' \sim 1$ (i.e. in the *sheared region*), due to the large magnetic shear and sufficiently weak pressure gradients (which are supposed to be localised within the low-shear region), mode coupling is prevented so that different Fourier harmonics behave independently. Moreover equilibrium flows effects are negligible, entering only in the definition of the Lagrangian displacement. Thus it is immediate to see that the leading contribution in (19) is due to the field line bending ($\boldsymbol{J}\times\boldsymbol{B}$) term, so that we write:

$$\boldsymbol{\nabla}(\boldsymbol{B}\cdot\boldsymbol{Q})+\boldsymbol{B}\cdot\boldsymbol{\nabla}\boldsymbol{Q}+\boldsymbol{Q}\cdot\boldsymbol{\nabla}\boldsymbol{B}=0.$$

By applying the operator $\hat{\boldsymbol{L}}$ on the equation above and selecting a generic Fourier mode ℓ, after some straightforward algebra the perturbation behaves according to the following expression [37]:

$$\frac{d}{dr}\left[r^3(\ell\mu-n)^2\frac{d\xi^r_\ell}{dr}\right]-r(m^2-1)(\ell\mu-n)^2\xi^r_\ell=0. \tag{24}$$

We now focus our analysis in the region where the safety factor is constant close to a rational number, i.e. $q=\frac{m}{n}-\delta q$ with $\delta q/q\sim\varepsilon$. It will be shown later that the derivation of the eigenmode equation for ξ^r_m requires the calculation of the $m\pm1$ component of the compressible part of the perturbed pressure, namely $\delta p_{m\pm1}$. First we note that equation (23) reduces to:

$$Q^\varphi_m=\frac{B_0}{R_0}\beta_0'\xi^r_m,$$

while higher order harmonics to the perturbed toroidal magnetic field are negligible. By means of (11) and (12) it follows that $(p\boldsymbol{\nabla}\cdot\boldsymbol{\xi})_{m\pm1}=p_0(\boldsymbol{\nabla}\cdot\boldsymbol{\xi})_{m\pm1}$, having used (21) for the main harmonic m. Hence using again the perpendicular incompressibility condition , i.e. Eq. (21) but this time specified for the $m\pm1$ modes, and exploiting the angular oscillation of the Jacobian (cf. (18)) the following expression is straightforwardly derived:

$$(p\boldsymbol{\nabla}\cdot\boldsymbol{\xi})_{m\pm1}=\pm p_0\left[i\frac{n}{m}\xi^\varphi_{m\pm1}-\frac{1}{mR_0}\left(r\frac{d\xi^r_m}{dr}+(1\mp m)\xi^r_m\right)\right]. \tag{25}$$

Thus from the equation above it is clear that an expression for the perturbed sideband toroidal displacement is needed. This is computed by projecting (20) along the equilibrium magnetic field and multiplying the result by $\sqrt{g}$ [34] (multiplying by the Jacobian is convenient because of the relation $(\sqrt{g}\boldsymbol{B}\cdot\boldsymbol{\nabla})_\ell=irB_0(\ell\mu-n)$). Eventually we obtain:

$$\frac{r(n\Omega_p\mp m\omega_D)^2\xi^\varphi_{m\pm1}}{\omega_A^2m^2}\pm i\Gamma\frac{nr}{m}\left(\tfrac{p}{B_0^2}\boldsymbol{\nabla}\cdot\boldsymbol{\xi}\right)_{m\pm1}=$$
$$\pm\frac{ir(\Omega+\Omega_p)[2m\omega_D\pm n(\Omega-\Omega_p)]}{2R_0\omega_A^2m^2}\left[r\frac{d\xi^r_m}{dr}+(1\mp m)\xi^r_m\right], \tag{26}$$

where $\omega_D=\omega+n\Omega$. Thus by combining (25) and (26) we finally obtain an expression for the parallel (i.e. in the $\boldsymbol{\nabla}\varphi$ direction) Lagrangian fluid displacement of the sideband harmonics:

$$\xi^\varphi_{m\pm1}=-\frac{i}{R_0}\frac{n\Gamma p_0\pm(\Omega+\Omega_p)[m\omega_D\pm n(\Omega-\Omega_p)/2]}{n^2\Gamma p_0-(n\Omega_p\mp m\omega_D)^2}\times$$
$$\times\left(r\frac{d\xi^r_m}{dr}+(1\mp m)\xi^r_m\right). \tag{27}$$

We point out that setting $\Omega_p=0$, the expression above recovers the result for $\xi^\varphi m\pm1$ obtained in Ref. [32]. We now proceed with the derivation of the eigenmode equations for $\xi^r_{m,m\pm1}$.

By applying the operator $\hat{\boldsymbol{L}}$ on (20) we explicitly obtain:

$$-\sqrt{g}\boldsymbol{\nabla}\varphi\cdot\boldsymbol{\nabla}\times\left(\frac{\boldsymbol{W}}{B^\varphi}\right)=[1/B^\varphi,\phi]$$
$$+\sqrt{g}\left(\boldsymbol{B}\cdot\boldsymbol{\nabla}\frac{\tilde{J}^\varphi}{B^\varphi}+\boldsymbol{Q}\cdot\boldsymbol{\nabla}\frac{J^\varphi}{B^\varphi}-\boldsymbol{J}\cdot\boldsymbol{\nabla}\frac{Q^\varphi}{B^\varphi}\right), \tag{28}$$

having introduced the notation $[a,b]=\partial_r a\partial_\vartheta b-\partial_\vartheta a\partial_r b$ and $\tilde{J}^\varphi=\frac{1}{\sqrt{g}}(\partial_rQ_\vartheta-\partial_\vartheta Q_r)$ with (cf. (19)):

$$\boldsymbol{W}=\rho\omega^2\boldsymbol{\xi}+2i\rho\omega\boldsymbol{v}\cdot\boldsymbol{\nabla}\boldsymbol{\xi}-\rho\boldsymbol{v}\cdot\boldsymbol{\nabla}[\boldsymbol{v}\cdot\boldsymbol{\nabla}\boldsymbol{\xi}]+\boldsymbol{\nabla}\cdot[\rho\boldsymbol{\xi}(\boldsymbol{v}\cdot\boldsymbol{\nabla})\boldsymbol{v}].$$

Equation (28) is the standard vorticity equation (see e.g. [34]) augmented by the helical flow terms. By selecting respectively the m and $m\pm1$ components, the corresponding coupled equations for the fluid displacements are obtained. These are derived in the next two subsections.

A. Harmonic m

Focussing on the mth harmonic of Eq. (28), a surprisingly long but straightforward manipulation gives (for sake of simplicity we assume that all the frequencies are normalised wrt ω_A, i.e. $(\omega,\Omega,\Omega_A)\to(\omega,\Omega,\Omega_A)/\omega_A$):

$$\frac{d}{dr}\left[r\left(A_+\xi^\varphi_{m+1}-A_-\xi^\varphi_{m-1}\right)\right]+m(A_+\xi^\varphi_{m+1}+A_-\xi^\varphi_{m-1})$$
$$-\{\sqrt{g}[1/B^\varphi_0,\Gamma p\boldsymbol{\nabla}\cdot\boldsymbol{\xi}]\}_m=\frac{i}{mR_0}\left\{\frac{1}{r}\frac{d}{dr}\left(r^3A_0\frac{d\xi^r_m}{dr}\right)\right.$$
$$+[(1-m^2)(A_0+r\Xi')+r\{\omega^2+2n\omega(\Omega+\Omega_p)\}'$$
$$+2rp'_\Omega(n^2-m^2)+\frac{2m^4R_0^2}{n^2}(p'_\Omega)^2]\xi^r_m$$
$$\left.+m^2R_0p'_\Omega\left[\frac{r^{-m-1}(r^{m+2}\xi^r_{m+1})'}{1+m}+\frac{r^{m-1}(r^{-m+2}\xi^r_{m-1})'}{1-m}\right]\right\}, \tag{29}$$

with $\Xi=(1+\frac{f}{2})(\Omega_p^2-\Omega^2)-\Gamma p_0f$, where we defined:

$$A_0=\omega_D^2+\Xi-n^2\left(\frac{\delta q}{q}\right)^2,$$
$$A_\pm=\left(\Omega+\Omega_p\right)\left[\omega_D\mp\frac{n}{2m}\left(\Omega_p-\Omega\right)\right].$$

Note that the lhs of (29) depends on the contravariant φ projection of the sidebands displacements which can be eliminated

by employing Eq. (27). Eventually we obtain the following equation for the main harmonic perturbation:

$$\frac{1}{r}\left(r^3 Q\frac{d\xi^r_m}{dr}\right) - (m^2-1)Q\xi^r_m + r\Big[\frac{i}{mR_0}\{\Xi+\omega^2+2n\omega(\Omega+\Omega_p) + 2\Gamma p_0\} + \frac{n\Gamma p_0}{m}\{g_+(1-m)+g_-(1+m)\} + \{B_+(1-m) - B_-(1+m)\}\Big]'\xi^r_m + \left(\frac{2ir}{mR_0}p'_\Omega(n^2-m^2) + \frac{2im^3R_0}{n}(p'_\Omega)^2\right)\xi^r_m + imp'_\Omega\left[\frac{r^{-m-1}(r^{m+2}\xi^r_{m+1})'}{1+m} + \frac{r^{m-1}(r^{-m+2}\xi^r_{m-1})'}{1-m}\right] = 0, \quad (30)$$

where we defined the following quantities:

$$Q = \tfrac{iA_0}{mR_0} - \tfrac{\Gamma p_0}{m}\left[2i/R_0 + n(g_+ + g_-) - (B_+ - B_-)\right],$$
$$g_\pm = -\frac{i(n\Gamma p_0 \pm mA_\pm)/R_0}{[n^2\Gamma p_0 - (m\omega_D \mp \Omega_p)^2]},$$
$$B_\pm = g_\pm A_\pm.$$

Equation (30) is the general eigenmode equation for the harmonic m, comprising coupling with the neighbouring sidebands, with the effects of helical flows. Note that to this order, both the toroidal and poloidal Mach numbers are assumed to be of the order of unity (with the constraint that $\mathcal{M}_p < 1$ to avoid shocks in the equilibrium density).

in order to have a simple analytic tractable model, the equation above can be further simplified by assuming that the frequencies associated with the equilibrium flow are sufficiently small compared to the sound speed (low-frequency limit), i.e. we let the Mach numbers to be small which is in accordance with experimental measurements. This is achieved by taking the limit $\Gamma \to \infty$. We may also assume that the flow enhancement of the pressure term can be neglected so that we shall approximate $p_\Omega \to p_0$. Thus by introducing the poloidal and toroidal rotation frequencies $V^P = \Omega_p$ and $V^T = \Omega + \Omega_p$ and restoring the Alfvén frequency $\omega_A = B_0/(R_0\sqrt{\rho})$ (we stress the point that the equilibrium mass density profile ρ depends upon r), in the limit the large sound speed to leading order in $1/\Gamma$ we obtain:

$$\frac{d}{dr}\left(r^3\hat{Q}_1\frac{d\xi^r_m}{dr}\right) - r\Big[(m^2-1)\hat{Q}_1 + r\hat{Q}'_2 + \frac{r}{R_0}\alpha(1-\tfrac{1}{q^2}) + \frac{\alpha^2}{2}\Big]\xi^r_m + \frac{\alpha}{2}\left[\frac{r^{-m}(r^{2+m}\xi^r_{m+1})'}{1+m} + \frac{r^m(r^{2-m}\xi^r_{m-1})'}{1-m}\right] = 0, \quad (31)$$

where $\hat{Q}_1 = \left(\frac{\delta q}{q}\right)^2 - \frac{(\omega+nV^T-mV^P)^2(1+2q^2)}{n^2\omega_A^2}$, $\hat{Q}_2 = [\omega^2(1+2q^2) + 2n\omega V^T]/(n^2\omega_A^2)$ and $\alpha = 2q^2R_0p'_0$. In the next subsection we will derive the equations for $\xi^r_{m\pm1}$ which are required to close the expression above.

B. Harmonics $m \pm 1$

The derivation of the sideband equations is simpler, because of the large parallel wave vector (i.e. $(m\pm1)\mu - n \sim 1$) which dominates over the inertial contribution. The helical flow effects in the $m \pm 1$ components of (28) enter only through a pressure enhancement factor which however can be dropped in the limit of large sound speed (viz. small Mach numbers). Hence the structure of the sideband equations is exactly the same as the one in Ref. [38]:

$$\left[r^{-1\mp2m}\left(r^{2\pm m}\xi^r_{m\pm1}\right)'\right]' = \frac{1\pm m}{2}\left[r^{\mp m}\alpha\xi^r_m\right]'. \quad (32)$$

In case of stronger flows, the equation for the sideband harmonics maintains the same structure of the expression above, where we only have to operate the substitution $\alpha \to \alpha_\Omega$.

Eventually the set of equations (24), (31) and (32) will be used in following section for the study of the stability of infernal-like perturbations in the edge pedestal (transport barrier) region. Although these are rather simplified (in particular concerning the strength of the helical flow) they are sufficiently general to provide a dispersion relation which can be used in a rather broad region in the parameters space. These equation are also suitable for the analysis of core transport barriers and this is reported in appendix B.

III. EDGE INFERNAL MODE ANALYSIS (ETB) WITH A SHEARED HELICAL FLOW

In this section we analyse the stability properties against infernal modes of a configuration which presents a flattening of the safety factor near the plasma edge (viz. occurring in the region $r_* < r < a$ where r_* is near the plasma boundary). We refer to the flat q region as the *weak shear region*. We also assume in this region the presence of strong pressure gradients. For sake of simplicity the pressure profile is chosen to be step-like, decreasing abruptly to zero at the middle point of the weak shear region (i.e. at $r_p = \frac{r_*+a}{2}$). Note that although we consider a case for which $\alpha \sim 1$, we nevertheless assume that the strong pressure gradient region is sufficiently narrow so that we can employ the expression of the metric tensor computed in the low β case (cf. (18)), and hence we can use Eqs. (31) and (32).

A similar configuration has been extensively analysed in Refs. [22, 23], here however the new ingredient entering in the following analysis is the presence of a sheared poloidal flow. We shall start the analysis by writing the eigenmode equations of the fluid displacement $\boldsymbol{\xi}$ for the main and sideband harmonics. Focussing first on the sidebands, integration of equation (32) yields:

$$L_\pm = r^{-1\mp2m}\left(r^{2\pm m}X_\pm\right)' - \frac{1\pm m}{2}\alpha r^{\mp m}\xi^r_m. \quad (33)$$

This equation is then plugged into (31) which yields [38–40]:

$$\frac{d}{dr}\left(r^3\hat{Q}_1\frac{d\xi^r_m}{dr}\right) - r\Big[(m^2-1)\hat{Q}_1 + r\hat{Q}'_2 + \frac{r\alpha}{R_0}\Big]\xi^r_m + \frac{\alpha}{2}\left[\frac{r^{1+m}L_+}{1+m} + \frac{r^{1-m}L_-}{1-m}\right] = 0, \quad (34)$$

where we have assumed that $q^2 \gg 1$. The dependence upon the sideband displacements appears implicitly through the two constants $L_\pm$. These are computed by first evaluating (33) at r_* and a providing the expression for $\xi^r_{m\pm1}$ at these two points respectively, and then integrating (33) from r_* to a [22]. Eventually we obtain:

$$\frac{L_\pm}{1 \pm m} = r_*^{-2\mp 2m}\Lambda^{(\pm)} \times \int_{r_*}^{a} \alpha r^{1\pm m}\xi^r_m dr, \tag{35}$$

where the explicit expression of $\Lambda^{(\pm)}$ reads [22]:

$$\Lambda^{(\pm)} = \frac{[2 \pm m + \mathbb{C}_\pm][2 \pm m + \mathbb{B}_\pm]}{(\mathbb{C}_\pm \mp m)[2 \pm m + \mathbb{B}_\pm] - (\mathbb{B}_\pm \mp m)[2 \pm m + \mathbb{C}_\pm]\left(\frac{a}{r_*}\right)^{2\pm 2m}},$$

with $\mathbb{C}_\pm = \frac{r d\xi^r_{m\pm1}/dr}{\xi^r_{m\pm1}}\Big|_{r_*}$ and $\mathbb{B}_\pm = \frac{r d\xi^r_{m\pm1}/dr}{\xi^r_{m\pm1}}\Big|_{a}$.

Therefore in order to compute $\Lambda^{(\pm)}$ we have to impose appropriate boundary conditions at r_* and a for the logarithmic derivatives of the sidebands displacements. In order to determine $\mathbb{C}_\pm$ we first solve $\xi^r_{m\pm1}$ in the region $0 < r < r_*$ (i.e. employing (24)) and then we impose smooth matching across r_*. Boundary conditions at the plasma edge depend on the plasma/outer world interface, e.g. the position of the wall of the vessel (including whether it is ideal or resistive), the separatrix and so on. Once the matching condition at a is given, the constants $L_\pm$ are completely determined. Since the main focus of this work is the effect on the stability of the sheared MHD poloidal flow, which enters only through the inertia of the main mode in the weak shear region, we may leave the boundary conditions of the sideband harmonics at the plasma boundary unspecified letting the analysis to be general. The expressions for $\mathbb{C}_\pm$ and $\mathbb{B}_\pm$ in the case of a limited plasma with an ideal or resistive wall at distance b from the plasma edge can be found in Refs. [22, 23]. Finally, the solution of (24) for the mth mode provides the appropriate boundary conditions at r_* and a, which read [22]:

$$\xi^r_m(r_*) = \xi^r_m(a) = 0. \tag{36}$$

The analysis is greatly simplified by choosing step profiles for equilibrium the mass density, pressure and toroidal flow which read:

$$p_0(r)/p_0(r_*) \sim \rho(r)/\rho(r_*) \sim V^T(r)/V^T(r_*) \sim \theta(r_p - r),$$

where $\theta(r)$ is the Heaviside step function of argument r. It is assumed that the mass density profile is constant all the way from the magnetic axis to r_p. Thus we denote with $\hat{\omega}_A$ the value (constant) of the Alfvén frequency on the magnetic axis.

Thus having determined the boundary conditions of the sideband harmonics at the boundary points of the weak-shear region, by means of the equilibrium profiles given above the dispersion relation is found by integrating equation (34) across r_p exploiting singularity in α due to the step in the pressure profile [22]. This procedure yields the following expression:

$$\frac{r_p[\![\hat{Q}_1 d\xi^r_m/dr]\!]_{r_p}}{\xi^r_m(r_p)} + \left(\frac{\omega^2(1+2q^2) + 2n\omega V^T}{n^2\hat{\omega}_A^2} - \hat{\beta}\right) + \frac{\hat{\beta}^2}{2\varepsilon_p^2}\left(\frac{r_p}{r_*}\right)^{2\pm 2m}\left[\Lambda^{(+)} + \Lambda^{(-)}\right] = 0,$$

with $\hat{\beta} = 2p_0(r_*)q^2/B_0^2$ and $[\![(\cdot)]\!]_{r_p} = [(\cdot)]^{r_p+\delta}_{r_p-\delta}$ with $\delta \to 0$ where continuity of ξ^r_m across r_p has been required (this is easily proved by a double integration firstly generic and then definite of (34) across r_p, i.e. in a neighbourhood of the pressure gradient). It can be shown that within the approximations employed in solving the dispersion relation, the second term in the left hand side of the equation above is negligible and thus it can be neglected. Thus the expression above can be recast as:

$$\frac{r_p[\![\hat{Q}_1 d\xi^r_m/dr]\!]_{r_p}}{\xi^r_m(r_p)} + \Lambda = 0, \tag{37}$$

where $\Lambda = \frac{\hat{\beta}^2}{2\varepsilon_p^2}\left(\frac{r_p}{r_*}\right)^{2\pm 2m}\left[\Lambda^{(+)} + \Lambda^{(-)}\right]$ measures the strength of the instability drive.

Hence in order to obtain the dispersion relation it remains to compute the radial derivatives of the main harmonic on the left and right of r_p. These quantities are obtained by solving equation (34) separately on the left and on the right of r_p with the requirement of ξ^r_m being continuous across this point. In general the factor $\hat{Q}_1$ has a complicated dependence upon the radial variable through the flow profile, hence a general exact expression for ξ^r_m cannot be found. There are however two cases in which a simple approximated solution for main harmonic can be found. In the first limit we assume that radial derivatives of the perturbed fluid displacement are much larger than m (*strong gradient limit*). In the second case we perform a WKB expansion for ξ^r_m regarding the number $1/m$ as a smallness parameter. These two limits are discussed in the next subsections.

A. Strong gradient limit

In the first case we assume that radial derivative of the perturbation are much larger than m, so that exploiting the step-like behaviour of the pressure profile, from Eq. (34), the resulting equation for ξ^r_m is:

$$\frac{d}{dr}\left(\hat{Q}_1 \frac{d\xi^r_m}{dr}\right) = 0,$$

which holds both for $r_* < r < r_p$ and for $r_p < r < a$ where $\hat{Q}$ has a radial dependence through the poloidal flow V^P. We point out that because of the step-like shape of the mass density entering in ω_A, inertial effects in the equation above enter only for $r < r_p$. We conveniently introduce the variable $x = (r - r_*)/(r_p - r_*) - 1$, and we choose a poloidal velocity profile in the region $r < r_p$ of the form $V^P = (1 + x)\bar{V}$ (note that $x = -1$ for $r = r_p$ and $x = 1$ for $r = a$). The shape of the profiles employed in this work are shown in figure 2.

Thus the solution of the equation above with vanishing boundary conditions at the edge of the weak-shear region

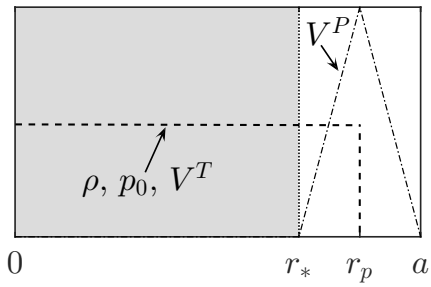

Figure 2. Example of the shape of the profiles used for the derivation of the dispersion relation (units are arbitrary). The grey shaded region is the high shear region.

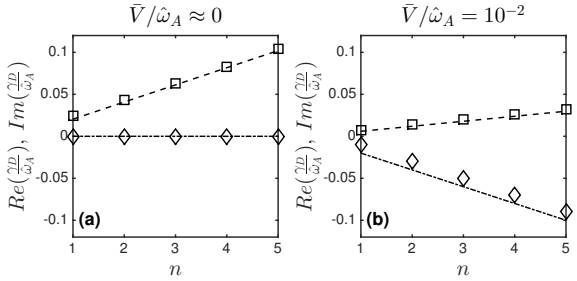

Figure 3. Plot of the growth rates $Re(\gamma_D)$ (squares from (40) and dashed line from (41)) and frequencies $Im(\gamma_D)$ (diamonds from (40) and dot-dashed line from (41)) with $q = 4$, $\delta q = 0.1$ and $\Lambda(r_p - r_*)/r_p = 0.015$ (supposed constant) for (a) $\bar{V} \approx 0$ and (b) $\bar{V} = 0.01$.

reads:

$$\xi_m^r = C\Bigg\{ \tanh^{-1}\left[\frac{\sqrt{1+2q^2}}{n\hat{\omega}_A\delta q/q}\left(\omega_D - m\bar{V}(1+x)\right)\right] - \tanh^{-1}\left(\frac{\omega_D\sqrt{1+2q^2}}{n\hat{\omega}_A\delta q/q}\right)\Bigg\}, \tag{38}$$

for $r_* < r < r_p$ where C is a generic constant, and

$$\xi_m^r = C\Bigg\{ \tanh^{-1}\left[\frac{\sqrt{1+2q^2}}{n\hat{\omega}_A\delta q/q}\left(m\bar{V} - \omega_D\right)\right] + \tanh^{-1}\left(\frac{\omega_D\sqrt{1+2q^2}}{n\hat{\omega}_A\delta q/q}\right)\Bigg\}(x-1), \tag{39}$$

for $r_p < r < a$. Note that continuity across r_p has been demanded.

Hence inserting the two expressions above into equation (37), the dispersion relation can be cast in the following form:

$$[Z(a_1,a_2)-1]-[a_1-a_2]^2 Z(a_1,a_2)+\frac{\Lambda(r_p-r_*)/r_p}{(\delta q/q)^2} = 0 \tag{40}$$

where $a_1 = \frac{\omega_D\sqrt{1+2q^2}}{n\hat{\omega}_A\delta q/q}$ and $a_2 = \frac{m\bar{V}\sqrt{1+2q^2}}{n\hat{\omega}_A\delta q/q}$ with:

$$Z(a_1,a_2) = \frac{a_2}{[1-(a_1-a_2)^2][\tanh^{-1}(a_1-a_2)-\tanh^{-1}(a_1)]}.$$

Generally speaking, equation (40) must be solved numerically. Nonetheless a rather simple explicit expression for the growth rate can be obtained by expanding the expression above to first order in $\bar{V}$. Hence we obtain ($\gamma_D = -i\omega_D$):

$$\frac{\gamma_D^2(1+2q^2)}{2n^2\hat{\omega}_A^2} + \left(\frac{\delta q}{q}\right)^2 - \frac{(r_p-r_*)\Lambda}{2r_p} + \frac{im\gamma_D\bar{V}(1+2q^2)}{2n^2\hat{\omega}_A^2} = 0,$$

whose solution reads:

$$\frac{\gamma_D}{\hat{\omega}_A} = -im\bar{V}/2 + \sqrt{\frac{2n^2}{1+2q^2}\left[\frac{(r_p-r_*)\Lambda}{2r_p} - \left(\frac{\delta q}{q}\right)^2\right] - \left(\frac{m\bar{V}}{2\hat{\omega}_A}\right)^2}. \tag{41}$$

The last term in the square root of the expression above provides the stabilising effect due to the poloidal flow. Since both the instability drive and the poloidal flow stabilising terms are increasing increases quadratically in n (and equivalently in m), we immediately recognise that the stabilisation is "*uniform*" in n, i.e. the stabilising effect enters only through a reduction of the slope of the growth rate when plotted against n. This is indeed well shown in Fig. 3, where the growth rates (and relative frequencies) computed by means of (40) and (41) are shown.

B. WKB (large m) limit

Analogously to the analysis of the previous section, we drop in equation (34) the terms proportional to α and $\hat{Q}_2$ (the latter because is proven to be negligible for localised modes). For sake of simplicity we rename $\hat{Q}_1 \to Q$. Hence the resulting equation reads [37]:

$$\frac{1}{r}\frac{d}{dr}\left[r^3 Q\frac{d\xi_m^r}{dr}\right] - (m^2-1)Q\xi_m^r = 0. \tag{42}$$

As before, we point out that inertial effects (i.e. Q) enter only for $r < r_p$ due to the step nature of the density profile. Thus introducing the smallness parameter $\delta = 1/m$ [41], the mode perturbation is then expanded within the WKB framework as:

$$\xi_m^r = \exp\left[\frac{1}{\delta}\sum_{k=0}^{\infty}\delta^k S_k(r)\right].$$

For sake of simplicity we assume that $rQ'/Q \ll 1/\delta$ (a WKB solution can be obtained for $rQ'/Q \sim 1/\delta$ which however contains integrals that must be evaluated numerically). Thus to leading order we have the WKB solution of (42) reads $\xi_m^r \propto r^{\pm m-1}/\sqrt{Q}$, so that imposing the boundary conditions given by Eq. (36) the perturbed fluid displacement of the main

harmonic m is:

$$\xi^r_m = \begin{cases} \sqrt{\dfrac{Q(r_p^-)}{Q(r)}}\left[\dfrac{\left(\frac{r}{r_*}\right)^{m-1}-\left(\frac{r}{r_*}\right)^{-m-1}}{\left(\frac{r_p}{r_*}\right)^{m-1}-\left(\frac{r_p}{r_*}\right)^{-m-1}}\right], & r<r_p, \\ \left[\dfrac{\left(\frac{r}{a}\right)^{m-1}-\left(\frac{r}{a}\right)^{-m-1}}{\left(\frac{r_p}{a}\right)^{m-1}-\left(\frac{r_p}{a}\right)^{-m-1}}\right], & r>r_p, \end{cases} \tag{43}$$

having normalised $\xi^r_m(r_p) = 1$.

Choosing a poloidal MHD flow profile of the form $V^P = \left(\frac{r_*-r}{r_*-r_p}\right)\bar{V}$ (similar to the one used in the previous analysis, see Fig. 2), we plug (43) into (37) which eventually gives:

$$\frac{(\omega_D - m\bar{V})}{\hat{\omega}_A^2}\left[(\omega_D - m\bar{V}) + \frac{mr_p\bar{V}}{(r_p - r_*)\mathfrak{G}}\right] + \frac{n^2}{(1+2q^2)}\left[\frac{\Lambda}{2\mathfrak{G}} - \left(\frac{\delta q}{q}\right)^2\right] = 0, \tag{44}$$

where we defined [22]:

$$\mathfrak{G} = -\frac{rd\xi^r_m/dr}{\xi^r_m}\Big|_{r_p^+} = \frac{m-1+(m+1)(r_*/r_p)^{2m}}{1-(r_*/r_p)^{2m}} > 0.$$

If the weak-shear region width is sufficiently narrow and m not dramatically large, we may approximate $\mathfrak{G} \approx 1/(r_p - r_*)$, hence the growth rate is eventually given by (41) and so regarding the growth behaviour and the stabilising effect of the sheared poloidal flow we arrive to the same conclusions drawn in the previous section (cf. figure 3). If m is increased and becomes sufficiently large compared to the weak-shear region width, we may approximate $\mathfrak{G} \sim m$. An immediate consequence is that for short wavelength modes (i.e. $m \gg (r_p - r_*)/a$) the sheared poloidal flow stabilisation effect is lost as clearly shown in Fig. 4. This is because the mode tends to become narrower and more localised when m is increased (cf. (43)), and in doing so the radial perturbation does not experience anymore the shearing of the poloidal flow, picking only the flow value at r_p.

IV. CONCLUSIONS

The impact of a subsonic helical MHD flow on the linear stability properties of a tokamak configuration against low-n perturbations radially localised over an extended weak-shear region has been assessed. First a Grad-Shafranov like equation, comprising poloidal and toroidal flow effects, has been solved by performing an ε expansion of the various equilibrium quantities. These have been used to compute the metric tensor up to order ε^2 under the assumption of small magnetic shear. By employing the infernal model, in which a dominant Fourier harmonic nearly resonant with the safety factor in the weak-shear region is coupled with its neighbouring sidebands, a set of three coupled differential equation has been derived. These have been obtained by performing a rigorous minimisation in the smallness parameter ε.

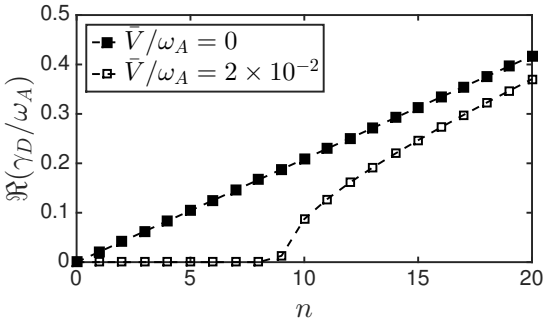

Figure 4. Plot of the growth rates $Re(\gamma_D)$ computed from (44) with $q = 4$, $\delta q = 0.1$, $r_* = 0.9$ and $\Lambda/2\mathfrak{G} = 0.015$ (assumed constant) for two different values of the poloidal flow strength. Note that modifying the amplitude of $\bar{V}$ we tune the shearing rate of the poloidal flow.

These equations have been consequently employed to derive analytically a dispersion relation which is function of plasma engineering parameters (e.g. q, β, etc.). Although such a dispersion relation has an implicit dependence upon the growth rate, a simple expression of the latter can be found in the limit of either large radial perturbation gradients or sufficiently large poloidal mode numbers. Boundary condition of the fluid perturbation between plasma and vacuum region have been left unspecified, so that the analysis can be generalised to various configurations (e.g. plasmas either limited or with separatrix, etc.). Assuming a constant instability drive, the results show that in both cases a reduction of the growth rate (i.e. stabilisation) is expected, although such a stabilising effect is *uniform* in n (or equivalently in m), viz. with a growth rate increasing with n the stabilising contribution increases with n as well. Moreover for sufficiently large m (i.e. for short wavelength modes) the stabilising effect of the sheared poloidal flow is lost and the perturbation experiences only a Doppler shift in its eigenfrequency. This suggests that a sheared poloidal alone is not sufficient, with the choice of the equilibrium profiles used in our analysis, to explain the complete stabilisation of short wavelength modes found experimentally.

Hence we infer that an additional physics ingredient which could have an important role in the determination of the stability properties should be the inclusion of finite Larmor radius effects in the pedestal region. Indeed large pressure gradients drive strong diamagnetic flows which could compete, in terms of order of magnitude, with the poloidal MHD flows. Current research is ongoing and new results will be presented in future papers.

We also point out that additional shaping effects, such as plasma elongation, which seems to favour the access to QH-regimes with edge mild MHD oscillations (namely EHOs), have been discarded in our analysis. Furthermore we stress that our model is extremely simplified. Indeed we account for a coupling of a reduced number of poloidal harmonics (in the infernal model actually three), whereas multiple poloidal modes all coupled together should be retained (analogously to

the ballooning theory). It is however envisaged that this problem can be tackled only numerically due to the complexity of the resulting equations. We finally point out that nonlinear dynamics may be crucial for the explanation of the appearance and evolution of such low-n modes, and this could stimulate the development of a *quasi-interchange*-like saturation model based on the work given in [42].

ACKNOWLEDGEMENTS

This work has been carried out within the framework of the EUROfusion Consortium and has received funding from the Euratom research and training programme 2014-2018 under grant agreement No 633053. The views and opinions expressed herein do not necessarily reflect those of the European Commission. This work was supported in part by the Swiss National Science Foundation.

Appendix A: Second order ε corrections to the metric tensor

In this appendix we report the higher order (to ε^2) corrections to the covariant metric tensor (18). We stress the point that the ε^2 expansion of the metric tensor is required to compute correctly the Christoffel symbols which enter in the projections of the momentum equation used for the eigenmode analysis. Hence the higher order ($\sim \varepsilon^2$) corrections to Eqs. (18) read:

$$
\begin{aligned}
g_{11} =& -\tfrac{r^2}{4R_0^2} - \tfrac{\Delta}{R_0} + \tfrac{r\Delta'}{R_0} + 2(\Delta')^2 \\
&- \left(\tfrac{r^2}{2R_0^2} + 2E' + \tfrac{2r}{R_0}\Delta' + (\Delta')^2\right)\cos 2\vartheta \\
&+ \left(\tfrac{2r^2\Delta''}{R_0} + 2r\Delta'\Delta'' + r^2(\Delta'')^2\right)\sin^2\vartheta, \\
g_{12} =& \left(\tfrac{r^3}{R_0^2} + \tfrac{9r^2}{4R_0}\Delta' + r(\Delta')^2 + \tfrac{5r^3}{4R_0}\Delta'' + \tfrac{3}{2}r^2\Delta'\Delta''\right. \\
&\left. + \tfrac{3}{2}E + \tfrac{r}{2}E' + \tfrac{r^2}{2}E''\right)\sin 2\vartheta, \\
g_{22} =& \tfrac{r^4}{4R_0^2} - \tfrac{r^2\Delta}{R_0} + \tfrac{r^3\Delta'}{R_0} + \tfrac{r^2}{2}(\Delta')^2 \\
&+ \left(\tfrac{3r^4}{2R_0^2} + 2r^2E' + \tfrac{4r^3}{R_0}\Delta' + \tfrac{5}{2}r^2(\Delta')^2\right)\cos 2\vartheta, \\
g_{33} =& -\tfrac{r^2}{2} - 2R_0\Delta + \tfrac{3}{2}r^2\cos 2\vartheta - 2rR_0\Delta'\sin^2\vartheta, \\
J_2 =& \tfrac{5r}{2R_0^3} + \tfrac{2\Delta}{rR_0^2} + \tfrac{r}{2R_0^3}\cos 2\vartheta + \tfrac{2\Delta'}{R_0^2}\sin^2\vartheta.
\end{aligned}
$$

Note that the contravariant coefficients of the metric tensor can be easily derived to second order from the expressions above.

Appendix B: Core infernal mode analysis (ITB) with constant flow

In this section we focus on a configuration which presents a strong pressure gradient in the core plasma within the region of the safety factor flattening which occurs for $r_1 < r < r_2$. In addition in this region equilibrium mass density, poloidal and toroidal rotations are assumed constant. This allows to treat Q as a constant and thus it can be moved outside the sign of derivation. Note also that no assumptions on the narrowness of the weak shear region are made, so that we may take the radial derivatives of the perturbation to be of order of unity. We point out that our analysis is similar to the one presented in Ref. [39] although in this reference the safety factor is taken non monotonic while in our analysis q increases with the minor radius (apart in the weak shear region in which it is assumed flat). We also allow the displacement for the main mode to be non top-hat (generally speaking a constant displacement would be more appropriate if a non monotonic safety factor drop well below the resonance which is crossed).

The equations that we are employ are (31) and (33) having set $\hat{Q}_2' = 0$ and renaming $\hat{Q}_1 \to Q$ [38–40]. By means of (33) we can reduce (31) to a form similar to (34) in which the Mercier contribution is given by $\frac{r\alpha}{R_0}(1 - 1/q^2)$. We assume that α is almost constant in the low shear region, viz. $p_0' \sim const$. Defining $D^{(\pm)} = \frac{\alpha}{2Q}\frac{L_\pm}{1\pm m}$, equation (34) can be cast in the following form:

$$
\begin{aligned}
&\frac{d}{dr}\left[r^3\frac{d\xi_m^r}{dr}\right] + r\left[(1-m^2) - Ar\right]\xi_m^r \\
&\quad + D^{(+)}r^{1+m} + D^{(-)}r^{1-m} = 0,
\end{aligned}
\tag{B1}
$$

where $A = \alpha/(R_0Q)(1 - 1/q^2)$. The solution of the equation above is:

$$
\begin{aligned}
\xi_m^r =& C_1\frac{K_{2m}(\varrho)}{r} + C_2\frac{I_{2m}(\varrho)}{r} + \\
&\tfrac{1}{A}[D^{(+)}r^{-1+m} + D^{(-)}r^{-1-m}],
\end{aligned}
\tag{B2}
$$

where K and I are the modified Bessel functions ([43] p. 355) and $\varrho = 2\sqrt{Ar}$.

The constants $L_\pm$ are given by (35) substituting $r_* \to r_1$ and $a \to r_2$. Hence the quantities $D^{(\pm)}$ are conveniently written as

$$
D^{(\pm)} = Z^{(\pm)}\int_{r_1}^{r_2} r^{1\pm m}\xi_m^r dr, \text{ with } Z^{(\pm)} = r_1^{-2\mp 2m}\left(\frac{\alpha^2}{2Q}\right)\Lambda^{(\pm)}.
$$

Following the approach adopted in Ref. [40], from the expressions above we can see that $D^{(\pm)}$ are *linear* in ξ_m^r, in particular we have $cD^{(-)}(\xi_m^r) = D^{(-)}(c\xi_m^r)$. Therefore we can rescale ξ_m^r dividing it by $D^{(+)}$. This leads to:

$$
\begin{aligned}
\xi_m^r/D^{(+)} =& C_1\frac{K_{2m}(\varrho)}{r} + C_2\frac{I_{2m}(\varrho)}{r} + \\
&\tfrac{1}{A}[r^{-1+m} + D^{(-)}(\xi_m^r/D^{(+)})r^{-1-m}],
\end{aligned}
\tag{B3}
$$

where we operated the substitution $C_1/D^{(+)} \to C_1$ and $C_2/D^{(+)} \to C_2$. Thus we immediately see that (B3) is equivalent to (B2) imposing the integral condition:

$$
D^{(+)} = 1. \tag{B4}
$$

There are four constants to be determined in expression (B2). The constants of integration C_1 and C_2 are found by imposing the boundary conditions for ξ_m^r at r_1 and r_2 (viz.

$\xi^r_m(r_1) = \xi^r_m(r_2) = 0$). The quantity $D^{(-)}$ is determined by multiplying (B3) by $Z^{(-)} \times r^{1-m}$ and integrating from r_1 to r_2 (having set $D^{(+)} = 1$), so that:

$$D^{(-)} = \frac{Z^{(-)} \int_{r_1}^{r_2} (H_- + {}^1/_A) dr}{1 - Z^{(-)} \int_{r_1}^{r_2} r^{-2m} dr}, \tag{B5}$$

where we introduced the function:

$$H_\pm = C_1 r^{\pm m} K_{2m}(\varrho) + C_2 r^{\pm m} I_{2m}(\varrho).$$

Note that the integrals in the expression above can be easily evaluated by exploiting the properties of the Bessel functions (see [43] p. 355) Using again (B2), the dispersion relation (B4) can be eventually written as:

$$Z^{(+)} \int_{r_1}^{r_2} \left[H_+ + \tfrac{1}{A}(r^{2m} + D^{(-)}) \right] dr = 1.$$

Since the dependence upon the growth rate, contained in Q, is embedded in the arguments of the Bessel functions, generally speaking this dispersion relation has to be solved numerically though some particular cases in which the dependence upon the growth rate becomes explicit may be identified.

[1] Zohm H 1996 *Plasma Phys. Control. Fusion* **38** 105
[2] Evans T E *et al.* 2004 *Phys. Rev. Lett.* **92** 235003
[3] Lang P T *et al.* 2008 *Nucl. Fusion* **48** 095007
[4] Burrell K H *et al.* 2002 *Plasma Phys. Control.Fusion* **44** A253
[5] Suttrop W *et al.* 2003 *PlasmaPhys. Control.Fusion* **45** 1399
[6] Burrell K H *et al.* 2005 *Phys. Plasmas* **12** 056121
[7] Greenfield C M *et al.* 2001 *Phys. Rev. Lett.* **86** 4544
[8] Suttrop W *et al.* 2004 *Plasma Phys. Control. Fusion* **46** A151
[9] Burrell K H *et al.* 2001 *Phys. Plasmas* **8** 2153
[10] Solano E *et al.* 2010 *Phys. Rev. Lett.* **104** 185003
[11] Burrell K H *et al.* 2009 *Nucl. Fusion* **49** 085024
[12] Connor J W *et al.* 1998 *Phys. Plasmas* **7** 2687
[13] Liu F *et al.* 2015 *Nucl. Fusion* **55** 113002
[14] Chen X *et al.* 2016 *Nucl. Fusion* **56** 076011
[15] Liu F *et al.* 2018 *Plasma Phys. Control. Fusion* **60** 014039
[16] Cooper W A *et al.* 2016 *Plasma Phys. Control. Fusion* **58** 064002
[17] Cooper W A *et al.* 2016 *Phys. Plasmas* **23** 040701
[18] Zheng L J *et al.* 2013 *Phys. Plasmas* **20** 012501
[19] Zheng L J *et al.* 2013 *Nucl. Fusion* **53** 063009
[20] Dong G Q *et al.* 2017 *Phys. Plasmas* **24** 112510
[21] Garofalo A M *et al.* 2015 *Phys. Plasmas* **22** 056116
[22] Brunetti D *et al.* 2018 *Nucl. Fusion* **58** 014002
[23] Brunetti D *et al.* 2018 *J. Plasma Phys.* **84** 745840201
[24] Hazeltine R D and Meiss J D 1992 *Plasma Confinement* (Redwood City: Addison-Wesley Publishing Company)
[25] Hameiri E 1983 *Phys. Fluids* **26** 230
[26] D'haeseleer W D *et al.* 1991 *Flux Coordinates and Magnetic Field Structure* (New York: Springer-Verlag)
[27] Burrell K *et al.* 2004 *Plasma Phys. Control. Fusion* **46** A165
[28] Hassam A B 1996 *Nucl. Fusion* **36** 707
[29] Greene J M *et al.* 1971 *Phys. Fluids* **14** 671
[30] Fitzpatrick R *et al.* 1993 *Nucl. Fusion* **33** 1533
[31] Wahlberg C and Bondeson A 2001 *Phys. Plasmas* **8** 3595
[32] Wahlberg C 2009 *Plasma Phys. Control. Fusion* **51** 085006
[33] Frieman E and Rotenberg M 1960 *Rev. Mod. Phys* **32** 898
[34] Mikhailovskii A B 1998 *Instabilities in a Confined Plasma* (Bristol: IOP)
[35] Glasser A H *et al.* 1975 *Phys. Fluids* **18** 875
[36] Coppi B *et al.* 1966 *Nucl. Fusion* **6** 101
[37] Newcomb W 1960 *Ann. Phys.* **10** 232
[38] Hastie R J and Hender T C 1988 *Nucl. Fusion* **28** 585
[39] Gimblett C G *et al.* 1996 *Phys. Plasmas* **3** 3369
[40] Wahlberg C and Graves J P 2007 *Phys. Plasmas* **14** 110703
[41] Hegna C C and Callen J D 1994 *Phys. Plasmas* **1** 2308
[42] Waelbroeck F L 1989 *Phys. Fluids B* **1** 499
[43] Abramowitz M and Stegun I 1968 *Handbook of Mathematical Functions With Formulas, Graphs, and Mathematical Tables* (New York: Dover)